High order finite difference WENO schemes for nonlinear degenerate parabolic equations

Yuanyuan Liu[1], Chi-Wang Shu[2] and Mengping Zhang[3]

Abstract

High order accurate weighted essentially non-oscillatory (WENO) schemes are usually designed to solve hyperbolic conservation laws or to discretize the first derivative convection terms in convection dominated partial differential equations. In this paper we discuss a high order WENO finite difference discretization for nonlinear degenerate parabolic equations which may contain discontinuous solutions. A porous medium equation is used as an example to demonstrate the algorithm structure and performance. Two different formulations of WENO schemes, one approximating directly the second derivative term using a conservative flux difference, and another approximating this term by first rewriting it as two first derivative terms using an auxiliary variable before applying the WENO procedure on those first derivatives, are discussed and compared. Numerical examples are provided to demonstrate the accuracy and non-oscillatory performance of these schemes.

Key Words: Weighted essentially non-oscillatory (WENO) scheme, finite difference scheme, nonlinear degenerate parabolic equation, porous medium equation

[1]Department of Mathematics, University of Science and Technology of China, Hefei, Anhui 230026, P.R. China. E-mail: xiaoliu@mail.ustc.edu.cn

[2]Division of Applied Mathematics, Brown University, Providence, RI 02912, USA. E-mail: shu@dam.brown.edu. Research supported by ARO grant W911NF-08-1-0520 and NSF grant DMS-0809086.

[3]Department of Mathematics, University of Science and Technology of China, Hefei, Anhui 230026, P.R. China. E-mail: mpzhang@ustc.edu.cn. Research supported by NSFC grant 10671190.

1 Introduction

Weighted essentially non-oscillatory (WENO) schemes were introduced in the literature to approximate hyperbolic conservation laws and the first derivative convection terms in convection dominated convection diffusion partial differential equations (PDEs). The first WENO scheme was introduced in 1994 by Liu, Osher and Chan in their pioneering paper [19], in which a third order accurate finite volume WENO scheme in one space dimension was constructed. In 1996, Jiang and Shu [15] provided a general framework to design arbitrary order accurate finite difference WENO schemes, which are more efficient for multi-dimensional calculations. Very high order WENO schemes are documented in [3]. All these papers use the WENO reconstruction procedure, which is equivalent to a conservative WENO approximation for the first derivative, and is the main relevant WENO procedure for designing both conservative finite volume and conservative finite difference schemes to solve hyperbolic conservation laws.

It was realized later that the WENO procedure can also be used in different contexts, for example in WENO interpolation and in WENO integration. The WENO interpolation procedure is used, for example, in [26] to transfer information from one domain to another in a high order, non-oscillatory fashion for a multi-domain WENO scheme, and in [6] to build a high order Lagrangian type method for solving Hamilton-Jacobi equations. The WENO integration procedure is used, for example, in [8, 9] for the design of high order residual distribution conservative finite difference WENO schemes. In our recent work [20] we have studied the positivity of linear weights for various WENO procedures, including reconstruction, interpolation, integration, and approximations to higher order derivatives. For an extensive review on WENO schemes, see [29].

In this paper, we are interested in designing WENO schemes for solving the following nonlinear, possibly degenerate parabolic equations

$$u_t = b(u)_{xx} \tag{1.1}$$

where $a(u) = b'(u) \geq 0$ and it is possible that $a(u) = 0$ for certain values of u. Such equations appear often in applications. For example, the following porous medium equation (PME) modelled in [22, 2]

$$u_t = (u^m)_{xx} \tag{1.2}$$

in which m is a constant greater than one, belongs to this class. This equation describes various diffusion processes, for example the flow of an isentropic gas through a porous medium, where u is the density of the gas required to be nonnegative and u^{m-1} is the pressure of the gas. Clearly, the equation degenerates at points where $u = 0$, resulting in the phenomenon of finite speed of propagation and discontinuous solutions.

The famous Barenblatt solution of the PME (1.2) is found in 1950 by Zel'dovich and Kompaneetz [31] (see also Barenblatt [4]), which is defined explicitly by

$$B_m(x,t) = t^{-k}\left[\left(1 - \frac{k(m-1)}{2m}\frac{|x|^2}{t^{2k}}\right)_+\right]^{1/(m-1)}, \qquad m > 1. \tag{1.3}$$

where $u_+ = \max(u, 0)$ and $k = (m+1)^{-1}$. This solution, for any time $t > 0$, has a compact support $[-\alpha_m(t), \alpha_m(t)]$ with the interface $|x| = \alpha_m(t)$ moving outward in a finite speed, where

$$\alpha_m(t) = \sqrt{\frac{2m}{k(m-1)}}\, t^k.$$

The Barenblatt solution shows that solutions to the PME may have the following properties:

1. Finite speed of propagation: If the initial function has compact support, then at all times the solution $u(\cdot, t)$ will have compact support.

2. Free-boundaries: The interface behaves like a free-boundary propagating with finite speed.

3. Weak solutions: Since there exists no derivative at the interface points $|x| = \alpha_m(t)$.

Various schemes for approximating (1.1) have been developed in the literature. Linear approximation schemes based on the nonlinear Chernoff's formula with a suitable

relaxation parameter have been studied in, e.g. [5, 23, 24, 21], where energy error estimates have also been investigated. See also [14, 16] for other types of linear approximation schemes. More recently, a different approach based on kinetic schemes for degenerate parabolic systems has been considered in [1]. Other approaches include that in [11], which is based on a suitable splitting technique with applications to more general hyperbolic-parabolic convection-diffusion equations, and that in [25], which is based on the maximum principle and on perturbation and regularization. A high order relaxation scheme has been presented in [7]. Finally a local discontinuous Galerkin finite element method has been constructed in [32] for the porous medium equation.

The degenerate parabolic equation (1.1) has similar features as a hyperbolic conservation law, such as the possible existence of discontinuous solutions and finite speed of propagation of wave fronts. Therefore, it is reasonable to generalize numerical techniques for solving hyperbolic conservation laws, such as the WENO technique, to solve the equation (1.1). This would involve a careful adaptation of the WENO procedure, to ensure conservation, accuracy and non-oscillatory performance. In this paper we discuss two different formulations of WENO schemes for approximating (1.1). The first formulation, discussed in Section 2, approximates directly the second derivative term using a conservative flux difference. This approach involves a narrower stencil for a given order of accuracy, however it would necessarily involve the usage of negative linear weights, therefore requiring a special treatment as in [27] to ensure non-oscillatory performance of the resulting WENO scheme. The second approach, discussed in Section 3, starts with the introduction of an auxiliary variable for the first derivative, then applies the WENO procedure to two first derivatives rather than to the second derivative term directly. This resembles the approach of the local discontinuous Galerkin method [10]. This approach requires only WENO approximations to first derivatives, which is a relatively mature procedure and avoids the appearance of negative linear weights. However, the computational cost is larger since two WENO approximations rather than one must be used

to approximate the second derivative. The effective stencil, which is a composition of two successive WENO procedures, is also wider in comparison with the first approach. We provide numerical examples to demonstrate the accuracy and non-oscillatory performance of these two types of WENO schemes and give a comparison.

2 Direct WENO discretization to the second derivative

In this section we study a direct WENO discretization to the second derivative in conservation form. Assume that we have a mesh $\cdots < x_1 < x_2 < x_3 < \cdots$, and for simplicity we assume the grid is uniform, i.e. $\Delta x = x_{i+1} - x_i$ is constant. We are building a conservative finite difference scheme for the equation (1.1), written in the form

$$\frac{du_i(t)}{dt} = \frac{\hat{f}_{i+\frac{1}{2}} - \hat{f}_{i-\frac{1}{2}}}{\Delta x^2}. \tag{2.1}$$

where $u_i(t)$ is the numerical approximation to the point value $u(x_i, t)$ of the solution to (1.1), and the numerical flux function

$$\hat{f}_{i+\frac{1}{2}} = \hat{f}(u_{i-r}, \ldots, u_{i+s}), \tag{2.2}$$

is chosen so that the conservative difference on the right hand side of the scheme (2.1) approximates the second order derivative $(b(u))_{xx}$ at $x = x_i$ to high order accuracy

$$\frac{\hat{f}_{i+\frac{1}{2}} - \hat{f}_{i-\frac{1}{2}}}{\Delta x^2} = (b(u))_{xx}|_{x=x_i} + O(\Delta x^k) \tag{2.3}$$

when the solution is smooth, and would generate non-oscillatory solutions when the solution contains possible discontinuities. The collection of grid points involved in the numerical flux (2.2), $S = \{x_{i-r}, \ldots, x_{i+s}\}$, is called the *stencil* of the flux approximation. A linear scheme is a scheme for which the numerical flux (2.2) is a linear combination of the grid values in the stencil

$$\hat{f}_{i+\frac{1}{2}} = \sum_{j=-r}^{s} a_j b(u_{i+j}). \tag{2.4}$$

where the constant coefficients a_j can be chosen to yield the highest order of accuracy k in (2.3). For example, the classical second order scheme

$$\frac{du_i(t)}{dt} = \frac{b(u_{i+1}) - 2b(u_i) + b(u_{i-1})}{\Delta x^2} \tag{2.5}$$

corresponds to the numerical flux with the stencil $S = \{x_i, x_{i+1}\}$ and is given by

$$\hat{f}_{i+\frac{1}{2}} = -b(u_i) + b(u_{i+1}).$$

The construction of WENO schemes in this section consists of the following steps.

1. We choose a symmetric *big stencil*, $S = \{x_{i-r}, \ldots, x_{i+r+1}\}$, for the numerical flux (2.4), resulting in a linear scheme with an order of accuracy $k = 2r + 2$ in (2.3). This linear scheme should be stable with the designed high order accuracy for smooth solutions, but will be oscillatory near discontinuities.

2. We choose s consecutive *small stencils*, $S^m = \{x_{i-r+m}, \ldots, x_{i+r+m+2-s}\}$, for $m = 0, \ldots, s-1$, resulting in a series of lower order linear schemes with their numerical fluxes denoted by $\hat{f}^{(m)}_{i+\frac{1}{2}}$. Here, s can be chosen to be between 2 and $2r+1$, corresponding to each small stencil containing $2r+1$ to 2 points, respectively.

3. We find the *linear weights*, namely constants d_m, such that the flux on the big stencil is a linear combination of the fluxes on the small stencils with d_m as the combination coefficients
$$\hat{f}_{i+\frac{1}{2}} = \sum_{m=0}^{s-1} d_m \hat{f}^{(m)}_{i+\frac{1}{2}}. \tag{2.6}$$
If we simply use the linear weights and linear combination on the right hand side of (2.6), we would get back the linear scheme on the big stencil, which will be accurate for smooth solutions but will be oscillatory near discontinuities.

4. We change the linear weights d_m in (2.6) to nonlinear weights ω_m, with the objective of maintaining the same high order accuracy for smooth solutions and non-oscillatory performance near discontinuities. This is usually achieved through

smoothness indicators which measure the smoothness of the function based on different small stencils.

If the linear weights d_m obtained in the third step above are non-negative, then the linear combination in (2.6) is a convex combination, since by consistency $\sum_{m=0}^{s-1} d_m = 1$. This will help significantly in the design of nonlinear weights in the fourth step above. In [20], we studied the positivity of linear weights for various WENO procedures. However, the current conservative approximation to the second derivative is not considered in [20]. We will therefore start with a discussion on the positivity of the linear weights below, with a rather disappointing conclusion that negative linear weights must appear.

2.1 Analysis of the linear weights

In this subsection we study the linear weights d_m in (2.6). In particular, we conclude that it is not possible to maintain all of them non-negative. We consider the cases of $r = 1$, 2 and 3, namely the big stencil containing 4, 6 and 8 points, corresponding to central schemes of fourth, sixth and eighth order accuracy, respectively.

The linear weights in (2.6), for various numbers of small stencils, are listed in Table 2.1. We conclude from this table that in some cases the linear weights do not exist for (2.6) to hold, and when they do exist, at least one of them is negative.

We give below the details for the situation $r = 2$, corresponding to 6 points in the big stencil, including the coefficients a_j in (2.4).

The big stencil in this case is given by

$$S = \{x_{i-2}, x_{i-1}, x_i, x_{i+1}, x_{i+2}, x_{i+3}\},$$

and the flux (2.4) corresponding to the big stencil is given by

$$\hat{f}_{i+\frac{1}{2}} = \frac{-2b(u_{i-2}) + 25b(u_{i-1}) - 245b(u_i) + 245b(u_{i+1}) - 25b(u_{i+2}) + 2b(u_{i+3})}{180},$$

corresponding to a sixth order central scheme. Depending on the number of small stencils, we have the following situations.

Table 2.1: Linear weights in (2.6). "—" represents the situation that linear weights do not exist.

number of nodes in the big stencil	number of nodes in each small stencil	linear weights
4	2	$d_0 = -\frac{1}{12},\ d_1 = \frac{7}{6},\ d_2 = -\frac{1}{12}.$
	3	——
6	2	$d_0 = \frac{1}{90},\ d_1 = -\frac{23}{180},\ d_2 = \frac{37}{30},$ $d_3 = -\frac{23}{180},\ d_4 = \frac{1}{90}.$
	3	——
	4	$d_0 = -\frac{2}{15},\ d_1 = \frac{19}{15},\ d_2 = -\frac{2}{15}.$
	5	——
8	2	$d_0 = -\frac{1}{560},\ d_1 = \frac{11}{504},\ d_2 = -\frac{779}{5040},$ $d_3 = \frac{533}{420},\ d_4 = -\frac{779}{5040},\ d_5 = \frac{11}{504},$ $d_6 = -\frac{1}{560}.$
	3	——
	4	$d_0 = -\frac{3}{1540}, d_1 = -\frac{226}{1155},\ d_2 = \frac{293}{210},$ $d_3 = -\frac{226}{1155},\ d_4 = -\frac{3}{1540}.$
	5	——
	6	$d_0 = -\frac{9}{56},\ d_1 = \frac{37}{28},\ d_2 = -\frac{9}{56}.$
	7	——

1. There are $s = 5$ small stencils and each small stencil consists of 2 points. The corresponding fluxes (2.4) are

$$\begin{aligned}
\hat{f}^{(0)}_{i+\frac{1}{2}} &= -b(u_{i-2}) + b(u_{i-1}), \quad \hat{f}^{(1)}_{i+\frac{1}{2}} = -b(u_{i-1}) + b(u_i), \quad \hat{f}^{(2)}_{i+\frac{1}{2}} = -b(u_i) + b(u_{i+1}),\\
\hat{f}^{(3)}_{i+\frac{1}{2}} &= -b(u_{i+1}) + b(u_{i+2}), \quad \hat{f}^{(4)}_{i+\frac{1}{2}} = -b(u_{i+2}) + b(u_{i+3}).
\end{aligned}$$

   The corresponding linear weights for (2.6) are

$$d_0 = \frac{1}{90}, \quad d_1 = -\frac{23}{180}, \quad d_2 = \frac{37}{30}, \quad d_3 = -\frac{23}{180}, \quad d_4 = \frac{1}{90}.$$

   Notice that d_1 and d_3 are negative.

2. There are $s = 4$ small stencils and each small stencil consists of 3 points. The corresponding fluxes (2.4) are

$$\begin{aligned}
\hat{f}^{(0)}_{i+\frac{1}{2}} &= b(u_{i-2}) - 3b(u_{i-1}) + 2b(u_i), \quad \hat{f}^{(1)}_{i+\frac{1}{2}} = -b(u_i) + b(u_{i+1}),\\
\hat{f}^{(2)}_{i+\frac{1}{2}} &= -b(u_i) + b(u_{i+1}), \qquad\qquad\qquad \hat{f}^{(3)}_{i+\frac{1}{2}} = -2b(u_{i+1}) + 3b(u_{i+2}) - b(u_{i+3}).
\end{aligned}$$

Unfortunately, in this case there does not exist a set of linear weights for (2.6) to hold.

3. There are $s = 3$ small stencils and each small stencil consists of 4 points. The corresponding fluxes (2.4) are

$$\begin{aligned}
\hat{f}^{(0)}_{i+\frac{1}{2}} &= \frac{b(u_{i-2}) - 3b(u_{i-1}) - 9b(u_i) + 11b(u_{i+1})}{12}, \\
\hat{f}^{(1)}_{i+\frac{1}{2}} &= \frac{b(u_{i-1}) - 15b(u_i) + 15b(u_{i+1}) - b(u_{i+2})}{12}, \\
\hat{f}^{(2)}_{i+\frac{1}{2}} &= \frac{-11b(u_i) + 9b(u_{i+1}) + 3b(u_{i+2}) - b(u_{i+3})}{12}.
\end{aligned}$$

The corresponding linear weights for (2.6) are

$$d_0 = -\frac{2}{15}, \quad d_1 = \frac{19}{15}, \quad d_2 = -\frac{2}{15}.$$

Notice that d_0 and d_2 are negative.

4. There are $s = 2$ small stencils and each small stencil consists of 5 points. The corresponding fluxes (2.4) are

$$\hat{f}^{(0)}_{i+\frac{1}{2}} = \hat{f}^{(1)}_{i+\frac{1}{2}} = b(u_{i-1}) - 15b(u_i) + 15b(u_{i+1}) - b(u_{i+2}).$$

In this case there does not exist a set of linear weights for (2.6) to hold.

2.2 Direct discretization on the big stencil with six uniform nodes

Based on the previous analysis of the linear weights, we consider the numerical flux $\hat{f}_{i+\frac{1}{2}}$ on the big stencil with six uniform nodes, that is $S = \{x_{i-2}, \ldots, x_{i+3}\}$, and choose the small stencils containing four uniform nodes, that is $S^m = \{x_{i-2+m}, \ldots, x_{i+1+m}\}$ with $m = 0, 1, 2$.

If we could find a function $h(x)$, which may depend on the grid size Δx, such that

$$b(u(x)) = \frac{1}{\Delta x^2} \int_{x-\frac{\Delta x}{2}}^{x+\frac{\Delta x}{2}} \left(\int_{\eta-\frac{\Delta x}{2}}^{\eta+\frac{\Delta x}{2}} h(\xi) d\xi \right) d\eta, \tag{2.7}$$

then clearly

$$(b(u))_{xx} = \frac{h(x+\Delta x) - 2h(x) + h(x-\Delta x)}{\Delta x^2}. \tag{2.8}$$

If we take the function

$$g(x) = h(x + \frac{\Delta x}{2}) - h(x - \frac{\Delta x}{2}), \tag{2.9}$$

we have

$$(b(u))_{xx}|_{x=x_i} = \frac{g(x_{i+\frac{1}{2}}) - g(x_{i-\frac{1}{2}})}{\Delta x^2}, \tag{2.10}$$

which involves no error in approximating the second order spatial derivative with a finite difference.

By approximating $g(x)$ in (2.9), conservative numerical schemes are formulated. These approximations of $g(x)$ are denoted by $p(x)$ and are constructed using a polynomial form with undetermined coefficients. We first consider a polynomial approximation to $h(x)$ of degree at most five on the big stencil S

$$h(x) \approx q(x) = a_0 + a_1 x + a_2 x^2 + a_3 x^3 + a_4 x^4 + a_5 x^5, \tag{2.11}$$

with undetermined coefficients a_k with $k = 0, \ldots, 5$. Substituting (2.11) into (2.7) and performing the integration gives

$$\begin{aligned} b(u(x)) &= a_0 + a_1 x + a_2 \left(x^2 + \frac{\Delta x^2}{6} \right) + a_3 \left(x^3 + \frac{\Delta x^2 x}{2} \right) + a_4 \left(x^4 + \Delta x^2 x^2 + \frac{\Delta x^4}{15} \right) \\ &\quad + a_5 \left(x^5 + \frac{5\Delta x^2 x^3}{3} + \frac{\Delta x^4 x}{3} \right). \end{aligned} \tag{2.12}$$

Given the point values of $b(u(x))$ on S, we have a system of six equations in the six unknown coefficients. Therefore the coefficients a_k can be solved explicitly (where $x_i = 0$):

$$\begin{aligned} a_0 &= \frac{1}{180} \left(2b(u_{i-2}) - 23b(u_{i-1}) + 222b(u_i) - 23b(u_{i+1}) + 2b(u_{i+2}) \right), \\ a_1 &= \frac{1}{120\Delta x} \left(8b(u_{i-2}) - 55b(u_{i-1}) - 70b(u_i) + 160b(u_{i+1}) - 50b(u_{i+2}) + 7b(u_{i+3}) \right), \\ a_2 &= \frac{1}{12\Delta x^2} \left(-b(u_{i-2}) + 10b(u_{i-1}) - 18b(u_i) + 10b(u_{i+1}) - b(u_{i+2}) \right), \\ a_3 &= \frac{1}{36\Delta x^3} \left(-b(u_{i-2}) - 4b(u_{i-1}) + 20b(u_i) - 26b(u_{i+1}) + 13b(u_{i+2}) - 2b(u_{i+3}) \right), \end{aligned}$$

$$
\begin{aligned}
a_4 &= \frac{1}{24\Delta x^4}\left(b(u_{i-2}) - 4b(u_{i-1}) + 6b(u_i) - 4b(u_{i+1}) + b(u_{i+2})\right), \\
a_5 &= \frac{1}{120\Delta x^5}\left(-b(u_{i-2}) + 5b(u_{i-1}) - 10b(u_i) + 10b(u_{i+1}) - 5b(u_{i+2}) + b(u_{i+3})\right).
\end{aligned}
$$

Substituting the coefficients into equation (2.11) gives the polynomial approximation to $g(x)$ of degree at most four

$$
\begin{aligned}
p(x) &= q\left(x + \frac{\Delta x}{2}\right) - q\left(x - \frac{\Delta x}{2}\right) \\
&= \frac{341b(u_{i-2}) - 2785b(u_{i-1}) - 2590b(u_i) + 6670b(u_{i+1}) - 1895b(u_{i+2}) + 259b(u_{i+3})}{5760} \\
&\quad + \left(\frac{-b(u_{i-2}) + 12b(u_{i-1}) - 22b(u_i) + 12b(u_{i+1}) - b(u_{i+2})}{8\Delta x}\right) x \\
&\quad + \left(\frac{-5b(u_{i-2}) - 11b(u_{i-1}) + 70b(u_i) - 94b(u_{i+1}) + 47b(u_{i+2}) - 7b(u_{i+3})}{48\Delta x^2}\right) x^2 \\
&\quad + \left(\frac{b(u_{i-2}) - 4b(u_{i-1}) + 6b(u_i) - 4b(u_{i+1}) + b(u_{i+2})}{6\Delta x^3}\right) x^3 \\
&\quad + \left(\frac{-b(u_{i-2}) + 5b(u_{i-1}) - 10b(u_i) + 10b(u_{i+1}) - 5b(u_{i+2}) + b(u_{i+3})}{24\Delta x^4}\right) x^4.
\end{aligned}
$$

Evaluating $p(x)$ at $x = x_{i+\frac{1}{2}}$, we finally obtain

$$
\begin{aligned}
\hat{f}_{i+\frac{1}{2}} &= p(x_{i+\frac{1}{2}}) \qquad (2.13) \\
&= \frac{-2b(u_{i-2}) + 25b(u_{i-1}) - 245b(u_i) + 245b(u_{i+1}) - 25b(u_{i+2}) + 2b(u_{i+3})}{180}.
\end{aligned}
$$

Notice that both x_i and Δx are not present in (2.13), therefore it is clear that the resulting stencil is independent of both and may be used to evaluate the numerical flux at any interface in the domain. From the definition (2.7) we also know that

$$
\begin{aligned}
\hat{f}_{i+\frac{1}{2}} = \frac{1}{180\Delta x^2} &\left(-2\int_{x_{i-\frac{5}{2}}}^{x_{i-\frac{3}{2}}}\left(\int_{\eta-\frac{\Delta x}{2}}^{\eta+\frac{\Delta x}{2}} h(\xi)d\xi\right)d\eta + 25\int_{x_{i-\frac{3}{2}}}^{x_{i-\frac{1}{2}}}\left(\int_{\eta-\frac{\Delta x}{2}}^{\eta+\frac{\Delta x}{2}} h(\xi)d\xi\right)d\eta\right. \\
&-245\int_{x_{i-\frac{1}{2}}}^{x_{i+\frac{1}{2}}}\left(\int_{\eta-\frac{\Delta x}{2}}^{\eta+\frac{\Delta x}{2}} h(\xi)d\xi\right)d\eta + 245\int_{x_{i+\frac{1}{2}}}^{x_{i+\frac{3}{2}}}\left(\int_{\eta-\frac{\Delta x}{2}}^{\eta+\frac{\Delta x}{2}} h(\xi)d\xi\right)d\eta \\
&\left.-25\int_{x_{i+\frac{3}{2}}}^{x_{i+\frac{5}{2}}}\left(\int_{\eta-\frac{\Delta x}{2}}^{\eta+\frac{\Delta x}{2}} h(\xi)d\xi\right)d\eta + 2\int_{x_{i+\frac{5}{2}}}^{x_{i+\frac{7}{2}}}\left(\int_{\eta-\frac{\Delta x}{2}}^{\eta+\frac{\Delta x}{2}} h(\xi)d\xi\right)d\eta\right).
\end{aligned}
$$

Substituting the Taylor series expansion at the grid point x_i

$$
h(\xi) = h(x_i) + \sum_{j=1}^{7}\frac{(\xi - x_i)^j}{j!}\frac{d^j h}{dx^j}|_{x=x_i} + O(\Delta x^8),
$$

and performing the integration, we have

$$\hat{f}_{i+\frac{1}{2}} = \sum_{j=1}^{6} \frac{\Delta x^j}{j!} \frac{d^j h}{dx^j}|_{x=x_i} + \frac{1}{504} \frac{d^7 h}{dx^7}|_{x=x_i} \Delta x^7 + O(\Delta x^8). \tag{2.14}$$

Compare (2.14) with the Taylor series expansion

$$\begin{aligned} g(x_{i+\frac{1}{2}}) &= h(x_{i+1}) - h(x_i) \\ &= \sum_{j=1}^{6} \frac{\Delta x^j}{j!} \frac{d^j h}{dx^j}|_{x=x_i} + \frac{1}{5040} \frac{d^7 h}{dx^7}|_{x=x_i} \Delta x^7 + O(\Delta x^8), \end{aligned} \tag{2.15}$$

we could obtain

$$\hat{f}_{i+\frac{1}{2}} = g(x_{i+\frac{1}{2}}) + \frac{1}{560} \frac{d^7 h}{dx^7}|_{x=x_i} \Delta x^7 + O(\Delta x^8). \tag{2.16}$$

Similarly we could calculate the numerical flux $\hat{f}_{i-\frac{1}{2}}$

$$\begin{aligned} \hat{f}_{i-\frac{1}{2}} &= \frac{-2b(u_{i-3}) + 25b(u_{i-2}) - 245b(u_{i-1}) + 245b(u_i) - 25b(u_{i+1}) + 2b(u_{i+2})}{180} \\ &= g(x_{i-\frac{1}{2}}) + \frac{1}{560} \frac{d^7 h}{dx^7}|_{x=x_i} \Delta x^7 + O(\Delta x^8). \end{aligned} \tag{2.17}$$

Therefore, substituting the equations (2.16) and (2.17) into the equation (2.10), we have

$$(b(u))_{xx}|_{x=x_i} = \frac{\hat{f}_{i+\frac{1}{2}} - \hat{f}_{i-\frac{1}{2}}}{\Delta x^2} + O(\Delta x^6). \tag{2.18}$$

Following a similar argument, we could obtain a different polynomial of degree at most two, denoted by $p_m(x)$, which approximates the function $g(x)$ in (2.10) on each small stencil $S^m = \{x_{i-2+m}, \ldots, x_{i+1+m}\}$ with $m = 0, 1, 2$.

$$\begin{aligned} p_0(x) &= \frac{5b(u_{i-2}) - 27b(u_{i-1}) + 15b(u_i) + 7b(u_{i+1})}{24} + \left(\frac{b(u_{i-1}) - 2b(u_i) + b(u_{i+1})}{\Delta x} \right) x \\ &\quad + \left(\frac{-b(u_{i-2}) + 3b(u_{i-1}) - 3b(u_i) + b(u_{i+1})}{\Delta x^2} \right) x^2, \\ p_1(x) &= \frac{-7b(u_{i-1}) - 15b(u_i) + 27b(u_{i+1}) - 5b(u_{i+2})}{24} + \left(\frac{b(u_{i-1}) - 2b(u_i) + b(u_{i+1})}{\Delta x} \right) x \\ &\quad + \left(\frac{-b(u_{i-1}) + 3b(u_i) - 3b(u_{i+1}) + b(u_{i+2})}{2\Delta x^2} \right) x^2, \\ p_2(x) &= \frac{-43b(u_i) + 69b(u_{i+1}) - 33b(u_{i+2}) + 7b(u_{i+3})}{24} \\ &\quad + \left(\frac{2b(u_i) - 5b(u_{i+1}) + 4b(u_{i+2}) - b(u_{i+3})}{\Delta x} \right) x \end{aligned} \tag{2.19}$$

$$+\left(\frac{-b(u_i)+3b(u_{i+1})-3b(u_{i+2})+b(u_{i+3})}{2\Delta x^2}\right)x^2.$$

The approximations are evaluated at the point $x_{i+\frac{1}{2}}$ to obtain the numerical fluxes on the small stencils $S^m=\{x_{i-2+m},\ldots,x_{i+1+m}\}$ with $m=0,1,2$:

$$\begin{aligned}
\hat{f}^{(0)}_{i+\frac{1}{2}} &= \frac{b(u_{i-2})-3b(u_{i-1})-9b(u_i)+11b(u_{i+1})}{12},\\
\hat{f}^{(1)}_{i+\frac{1}{2}} &= \frac{b(u_{i-1})-15b(u_i)+15b(u_{i+1})-b(u_{i+2})}{12},\\
\hat{f}^{(2)}_{i+\frac{1}{2}} &= \frac{-11b(u_i)+9b(u_{i+1})+3b(u_{i+2})-b(u_{i+3})}{12}.
\end{aligned} \tag{2.20}$$

We only need to shift each index by -1 to obtain the flux $\hat{f}^{(m)}_{i-\frac{1}{2}}$. Hence the Taylor series expansions of (2.20) give

$$\begin{aligned}
\hat{f}^{(0)}_{i\pm\frac{1}{2}} &= g(x_{i\pm\frac{1}{2}})+\frac{1}{12}\frac{d^4h}{dx^4}|_{x=x_i}\Delta x^4+O(\Delta x^5),\\
\hat{f}^{(1)}_{i\pm\frac{1}{2}} &= g(x_{i\pm\frac{1}{2}})-\frac{1}{90}\frac{d^5h}{dx^5}|_{x=x_i}\Delta x^5+O(\Delta x^6),\\
\hat{f}^{(2)}_{i\pm\frac{1}{2}} &= g(x_{i\pm\frac{1}{2}})-\frac{1}{12}\frac{d^4h}{dx^4}|_{x=x_i}\Delta x^4+O(\Delta x^5),
\end{aligned} \tag{2.21}$$

and the finite difference approximations

$$\begin{aligned}
(b(u))_{xx}|_{x=x_i} &= \frac{\hat{f}^{(0)}_{i+\frac{1}{2}}-\hat{f}^{(0)}_{i-\frac{1}{2}}}{\Delta x^2}+O(\Delta x^3),\\
(b(u))_{xx}|_{x=x_i} &= \frac{\hat{f}^{(1)}_{i+\frac{1}{2}}-\hat{f}^{(1)}_{i-\frac{1}{2}}}{\Delta x^2}+O(\Delta x^4),\\
(b(u))_{xx}|_{x=x_i} &= \frac{\hat{f}^{(2)}_{i+\frac{1}{2}}-\hat{f}^{(2)}_{i-\frac{1}{2}}}{\Delta x^2}+O(\Delta x^3).
\end{aligned} \tag{2.22}$$

We could also obtain the linear weights

$$d_0=-\frac{2}{15},\qquad d_1=\frac{19}{15},\qquad d_2=-\frac{2}{15}, \tag{2.23}$$

satisfying

$$\hat{f}_{i+\frac{1}{2}}=\sum_{m=0}^{2}d_m\ \hat{f}^{(m)}_{i+\frac{1}{2}}$$

where $\hat{f}_{i+\frac{1}{2}}$ and $\hat{f}^{(m)}_{i+\frac{1}{2}}$ are given in (2.13) and (2.20) respectively.

2.2.1 A technique of treating negative weights

We could use the technique in [27] to treat the negative weights in (2.23). We split the linear weights into two parts: positive and negative by defining

$$\tilde{\gamma}_m^+ = \frac{1}{2}(d_m + \theta|d_m|), \quad \tilde{\gamma}_m^- = \tilde{\gamma}_m^+ - d_m, \quad m = 0, 1, 2,$$

where $\theta = 3$. Then we obtain

$$\begin{aligned} \tilde{\gamma}_0^+ &= \frac{2}{15}, \qquad \tilde{\gamma}_1^+ = \frac{38}{15}, \qquad \tilde{\gamma}_2^+ = \frac{2}{15}; \\ \tilde{\gamma}_0^- &= \frac{4}{15}, \qquad \tilde{\gamma}_1^- = \frac{19}{15}, \qquad \tilde{\gamma}_2^- = \frac{4}{15}. \end{aligned}$$

We scale them by

$$\sigma^+ = \sum_{m=0}^{2} \tilde{\gamma}_m^+ = \frac{42}{15}, \quad \sigma^- = \sum_{m=0}^{2} \tilde{\gamma}_m^- = \frac{27}{15}, \tag{2.24}$$

and obtain the linear weights of the two parts by $\gamma_m^\pm = \tilde{\gamma}_m^\pm / \sigma^\pm$ with $m = 0, 1, 2$:

$$\gamma_0^+ = \frac{1}{21}, \qquad \gamma_1^+ = \frac{19}{21}, \qquad \gamma_2^+ = \frac{1}{21}; \tag{2.25}$$

$$\gamma_0^- = \frac{4}{27}, \qquad \gamma_1^- = \frac{19}{27}, \qquad \gamma_2^- = \frac{4}{27}. \tag{2.26}$$

It is easy to check that

$$\sum_{m=0}^{2} \gamma_m^\pm = 1, \quad \text{and} \quad d_m = \sigma^+ \gamma_m^+ - \sigma^- \gamma_m^-. \tag{2.27}$$

2.2.2 The smoothness indicators and the nonlinear weights

To change the linear weights to nonlinear weights, we use the definition of the smoothness function in the paper [15, 28]

$$\beta_m = \sum_{l=1}^{2} \Delta x^{2l-1} \int_{x_i}^{x_{i+1}} \left(\frac{d^l}{dx^l} p_m(x) \right)^2 dx, \tag{2.28}$$

where the approximation polynomials $p_m(x)$ on the small stencils $S^m = \{x_{i-2+m}, \ldots, x_{i+1+m}\}$ with $m = 0, 1, 2$ are given in (2.19), and obtain the smoothness indicators

$$\beta_0 \;=\; \frac{13}{12}(b(u_{i-2}) - 3b(u_{i-1}) + 3b(u_i) - b(u_{i+1}))^2$$

$$
\begin{aligned}
&+\frac{1}{4}(b(u_{i-2})-5b(u_{i-1})+7b(u_i)-3b(u_{i+1}))^2,\\
\beta_1 &= \frac{13}{12}(b(u_{i-1})-3b(u_i)+3b(u_{i+1})-b(u_{i+2}))^2\\
&+\frac{1}{4}(b(u_{i-1})-b(u_i)-b(u_{i+1})+b(u_{i+2}))^2, \qquad (2.29)\\
\beta_2 &= \frac{13}{12}(b(u_i)-3b(u_{i+1})+3b(u_{i+2})-b(u_{i+3}))^2\\
&+\frac{1}{4}(-3b(u_i)+7b(u_{i+1})-5b(u_{i+2})+b(u_{i+3}))^2.
\end{aligned}
$$

Here we perform the integration over the interval $[x_i, x_{i+1}]$ to satisfy the symmetry property of the parabolic equation, and the factor Δx^{2l-1} in (2.28) is introduced to remove any Δx dependency in the final expression of the smoothness indicators in (2.29).

For the positive and negative linear weights $\gamma_m^{\pm}$ in (2.25) and (2.26), we define the nonlinear weights for the positive and negative groups $\tilde{\omega}_m^{\pm}$ respectively, denoted by $\omega_m^{\pm}$, based on the same smoothness indicators β_m given in (2.29)

$$
\omega_m^{\pm} = \frac{\tilde{\omega}_m^{\pm}}{\sum_{l=0}^{2}\tilde{\omega}_l^{\pm}}, \qquad \tilde{\omega}_m^{\pm} = \frac{\gamma_m^{\pm}}{(\epsilon+\beta_m)^2}, \qquad m=0,1,2, \qquad (2.30)
$$

where ϵ is to avoid the denominator to become zero, in this paper we take $\epsilon = 10^{-6}$. It is easy to verify $\sum_{m=0}^{2}\omega_m^{\pm} = 1$.

2.2.3 The finite difference WENO scheme

Rewrite the positive and negative nonlinear weights in (2.30) together, we finally obtain the nonlinear weights

$$
\omega_m = \sigma^{+}\omega_m^{+} - \sigma^{-}\omega_m^{-} \qquad (2.31)
$$

with $\sigma^{\pm}$ given in (2.24), and the WENO approximation flux

$$
\hat{f}_{i+\frac{1}{2}} = \sum_{m=0}^{2}\omega_m \hat{f}_{i+\frac{1}{2}}^{(m)} \qquad (2.32)
$$

where $\hat{f}_{i+\frac{1}{2}}^{(m)}$ with $m=0,1,2$ are given by (2.20).

Then the semi-discrete finite difference WENO scheme could be expressed as

$$
\frac{du_i(t)}{dt} = \frac{\hat{f}_{i+\frac{1}{2}} - \hat{f}_{i-\frac{1}{2}}}{\Delta x^2}. \qquad (2.33)
$$

2.2.4 Runge-Kutta time discretization

Up to now we have only considered spatial discretization, leaving the time variable continuous. After the spatial discretization, the semi-discrete finite difference WENO scheme is equivalent to the first-order ODE system:

$$\frac{du(t)}{dt} = L(u) \tag{2.34}$$

where $L(u)$ results from the right hand side of (2.33).

In this paper, we use the third-order TVD Runge-Kutta method [30] to solve (2.34), which is given by

$$\begin{aligned} u^{(1)} &= u^n + \Delta t L(u^n), \\ u^{(2)} &= \frac{3}{4}u^n + \frac{1}{4}u^{(1)} + \frac{1}{4}\Delta t L(u^{(1)}), \\ u^{(3)} &= \frac{1}{3}u^n + \frac{2}{3}u^{(2)} + \frac{2}{3}\Delta t L(u^{(2)}). \end{aligned}$$

2.3 Analysis of the accuracy of the finite difference WENO scheme

In order to achieve the objective of maintaining the same high order accuracy as in (2.18) in smooth regions and non-oscillatory performance in regions where a discontinuity does exist, we need to find out the accuracy requirement of the finite difference WENO scheme (2.33).

Adding and subtracting $\sum_{m=0}^{2} \mathrm{d}_m \hat{f}^{(m)}_{i+\frac{1}{2}}$ from (2.32) gives

$$\hat{f}_{i+\frac{1}{2}} = \sum_{m=0}^{2} \mathrm{d}_m \hat{f}^{(m)}_{i+\frac{1}{2}} + \sum_{m=0}^{2} (\omega_m - d_m) \hat{f}^{(m)}_{i+\frac{1}{2}}. \tag{2.35}$$

Then we have

$$\hat{f}_{i+\frac{1}{2}} - \hat{f}_{i-\frac{1}{2}} = \sum_{m=0}^{2} \mathrm{d}_m \hat{f}^{(m)}_{i+\frac{1}{2}} - \sum_{m=0}^{2} \mathrm{d}_m \hat{f}^{(m)}_{i-\frac{1}{2}} + \sum_{m=0}^{2} (\omega_m^{(+)} - d_m) \hat{f}^{(m)}_{i+\frac{1}{2}} - \sum_{m=0}^{2} (\omega_m^{(-)} - d_m) \hat{f}^{(m)}_{i-\frac{1}{2}}, \tag{2.36}$$

where the superscript $(+)$ or $(-)$ on ω_m indicate their use in the stencil of either $\hat{f}_{i+\frac{1}{2}}$ or $\hat{f}_{i-\frac{1}{2}}$. From equations (2.16), (2.17) and (2.18), the first two terms are

$$\sum_{m=0}^{2} \mathrm{d}_m \hat{f}_{i+\frac{1}{2}}^{(m)} - \sum_{m=0}^{2} \mathrm{d}_m \hat{f}_{i-\frac{1}{2}}^{(m)} = (b(u))_{xx}|_{x=x_i} \Delta x^2 + O(\Delta x^8). \tag{2.37}$$

We expand the last two terms in (2.36), substituting for $\hat{f}_{i\pm\frac{1}{2}}^{(m)}$ from (2.21), and noticing that $\sum_{m=0}^{2} d_m = \sum_{m=0}^{2} \omega_m = 1$. Finally we obtain the necessary and sufficient conditions to achieve sixth-order accuracy convergence

$$(\omega_0^{(+)} - \omega_0^{(-)} - \omega_2^{(+)} + \omega_2^{(-)}) = O(\Delta x^4), \tag{2.38}$$

$$(\omega_m - d_m) = O(\Delta x^3). \tag{2.39}$$

Here we drop the superscript $(\pm)$ because (2.38) and (2.39) constrain both the "+" and "-" stencils. (2.39) gives us a simple set of criteria around which to design the nonlinear weights ω_m; while (2.38) is a difficult constraint to use in the design of the nonlinear weights.

Therefore in order to satisfy the condition (2.39), we have to analyze the nonlinear weights from (2.31). First we will consider the smoothness indicators β_m with $m = 0, 1, 2$.

2.3.1 The analysis of the smoothness indicators

Expand the smoothness indicators β_m (2.29) with $m = 0, 1, 2$ at the grid point x_i

$$\begin{aligned}
\beta_0 &= b_{xx}^2 \Delta x^4 + b_{xx}^2 b_{xxx} \Delta x^5 + \frac{1}{3}(4b_{xxx}^2 - b_{xx} b_{xxxx}) \Delta x^6 + O(\Delta x^7), \\
\beta_1 &= b_{xx}^2 \Delta x^4 + b_{xx}^2 b_{xxx} \Delta x^5 + \frac{2}{3}(2b_{xxx}^2 + b_{xx} b_{xxxx}) \Delta x^6 + O(\Delta x^7), \\
\beta_2 &= b_{xx}^2 \Delta x^4 + b_{xx}^2 b_{xxx} \Delta x^5 + \frac{1}{3}(4b_{xxx}^2 - b_{xx} b_{xxxx}) \Delta x^6 + O(\Delta x^7).
\end{aligned}$$

Therefore if

1. $b_{xx} \neq 0$, we have $\beta_m = D(1 + O(\Delta x))$ with $m = 0, 1, 2$;

2. $b_{xx} = 0, b_{xxx} \neq 0$, we have $\beta_m = D(1 + O(\Delta x))$ with $m = 0, 1, 2$.

where D is a nonzero quantity independent of m (but may depend on the derivatives of $b(u(x))$ and Δx). From the previous analysis we have

$$\beta_m = D(1 + O(\Delta x)), \qquad m = 0, 1, 2. \tag{2.40}$$

2.3.2 The relationship between β_m, γ_m and ω_m

Through a Taylor expansion analysis, we conclude that $\beta_m = D(1 + O(\Delta x^{k-1}))$ is the sufficient condition so that $\omega_m = \mathrm{d}_m + O(\Delta x^{k-1})$ holds, where D is a nonzero quantity independent of m (but may depend on Δx).

Because of the Taylor expansion $\frac{1}{(1+x)^2} = 1 - 2x + 3x^2 \cdots$ near $x = 0$ and neglecting ϵ, we could obtain

$$\frac{\gamma_m^{\pm}}{(\epsilon + \beta_m)^2} = \frac{\gamma_m^{\pm}}{(D(1 + O(\Delta x^{k-1})))^2} = \frac{\gamma_m^{\pm}}{D^2}(1 + O(\Delta x^{k-1})).$$

From the definition of the nonlinear weights in (2.30) and $\sum_{m=0}^{2} \gamma_m^{\pm} = 1$, we have

$$\begin{aligned} \gamma_m^{\pm} &= \omega_m^{\pm} \left(\sum_{l=0}^{2} \frac{\gamma_l^{\pm}}{(\epsilon + \beta_l)^2} \right) (\epsilon + \beta_m)^2, \\ &= \omega_m^{\pm} \left(\frac{1}{D^2}(1 + O(\Delta x^{k-1})) \right) (D(1 + O(\Delta x^{k-1})))^2, \\ &= \omega_m^{\pm} + O(\Delta x^{k-1}), \qquad m = 0, 1, 2. \end{aligned} \tag{2.41}$$

Thus through the previous analysis, the conditions (2.27), (2.40) and (2.41) imply that the nonlinear weights defined in (2.30) and (2.31) are given by

$$\omega_m = d_m + O(\Delta x), \qquad m = 0, 1, 2. \tag{2.42}$$

Unfortunately, in this case the condition (2.39) is not satisfied, that is, we can not achieve the sixth order accuracy by only using the nonlinear weights defined in (2.30) and (2.31).

2.3.3 Mapped nonlinear weights

To increase the accuracy of the nonlinear weights, we use the mapped function introduced in [13]

$$\mathrm{g}_m(\omega) = \frac{\omega(d_m + d_m^2 - 3d_m\omega + \omega^2)}{d_m^2 + \omega(1 - 2d_m)}, \quad m = 0, 1, 2. \tag{2.43}$$

This function is monotonically increasing with a finite slope, $\mathrm{g}_m(0) = 0$, $\mathrm{g}_m(1) = 1$, $\mathrm{g}_m(d_m) = d_m$, $\mathrm{g}_m^{'}(d_m) = 0$ and $\mathrm{g}_m^{''}(d_m) = 0$. The mapped nonlinear weights are given by

$$\alpha_m = \mathrm{g}_m(\omega_m), \qquad m = 0, 1, 2, \tag{2.44}$$

where d_m and ω_m are computed in (2.23), (2.30) and (2.31) respectively.

The mapped nonlinear weights are then defined as follows

$$\omega_m^{(M)} = \frac{\alpha_m}{\sum_{m=0}^{2} \alpha_m}, \qquad m = 0, 1, 2. \tag{2.45}$$

Hence the final form of the semi-discrete finite difference mapped WENO scheme is

$$\frac{du_i(t)}{dt} = \frac{\hat{f}_{i+\frac{1}{2}} - \hat{f}_{i-\frac{1}{2}}}{\Delta x^2}, \tag{2.46}$$

with the approximation flux

$$\hat{f}_{i+\frac{1}{2}} = \sum_{m=0}^{2} \omega_m^{(M)} \hat{f}_{i+\frac{1}{2}}^{(m)}, \tag{2.47}$$

where $\hat{f}_{i+\frac{1}{2}}^{(m)}$ with $m = 0, 1, 2$ are given by (2.20).

By Taylor series approximation of the $\mathrm{g}_m(\omega)$ at d_m and the condition (2.42) we have

$$\begin{aligned} \alpha_m &= \mathrm{g}_m(d_m) + \mathrm{g}_m^{'}(d_m)(\omega_m - d_m) + \frac{\mathrm{g}_m^{''}(d_m)}{2}(\omega_m - d_m)^2 + \frac{\mathrm{g}_m^{'''}(d_m)}{6}(\omega_m - d_m)^3 + \cdots \\ &= d_m + \frac{(\omega_m - d_m)^3}{d_m - d_m^2} + \cdots \\ &= d_m + O(\Delta x^3), \end{aligned} \tag{2.48}$$

and then

$$\omega_m^{(M)} = (d_m + O(\Delta x^3))(1 + O(\Delta x^3)) = d_m + O(\Delta x^3), \quad m = 0, 1, 2, \tag{2.49}$$

because of $\sum_{m=0}^{2} d_m = 1$. Now the condition (2.39) is satisfied, therefore the mapped WENO scheme (2.46) has the sixth order accuracy for smooth solutions and is non-oscillatory near discontinuities as verified by numerical experiments given later.

2.4 Numerical results

Example 1. We first test the accuracy of the finite difference WENO scheme (2.46) for the case $m = 1$ in (1.2), that is the linear initial value problem

$$\begin{cases} u_t = u_{xx}, \\ u(x,0) = \sin(x). \quad -\pi \le x \le \pi \end{cases} \tag{2.50}$$

on the big stencil $S = \{x_{i-2}, \ldots, x_{i+3}\}$ and the small stencils $S_m = \{x_{i-2+m}, \ldots, x_{i+1+m}\}$ with $m = 0, 1, 2$. It is easy to verify that the exact solution of the problem (2.50) is

$$u(x,t) = e^{-t}\sin(x).$$

In Table 2.2 we show the results of the sixth order mapped WENO scheme (2.46), at the final time $T = 2$ with periodic boundary condition.

Table 2.2: Accuracy on $u_t = u_{xx}$ with $u(x,0) = \sin(x)$

N	L^1 error	order	L^∞ error	order
10	1.50E-04	–	3.74E-05	–
20	1.87E-06	6.32	4.74E-07	6.30
40	2.81E-08	6.05	7.05E-09	6.07
80	4.39E-10	6.00	1.10E-10	6.00
160	6.93E-12	5.99	1.73E-12	5.99
320	5.66E-14	6.94	1.82E-14	6.57

We can see that the sixth order finite difference mapped WENO scheme (2.46) gives the expected order of accuracy.

Example 2. Then we begin our simulation for the Barenblatt solution given in (1.3) for the PME (1.2), where the initial condition is taken as the Barenblatt solution at $t = 1$, and the boundary condition is $u(\pm 6, t) = 0$ for $t > 1$.

We divide the computational domain into $N = 160$ uniform cells, and plot the numerical solution at $T = 2$ respectively for $m = 2, 3, 5$ and 8. The results are shown in Figure 2.1, in which the circle-box is the numerical solution and the solid line is the exact solution.

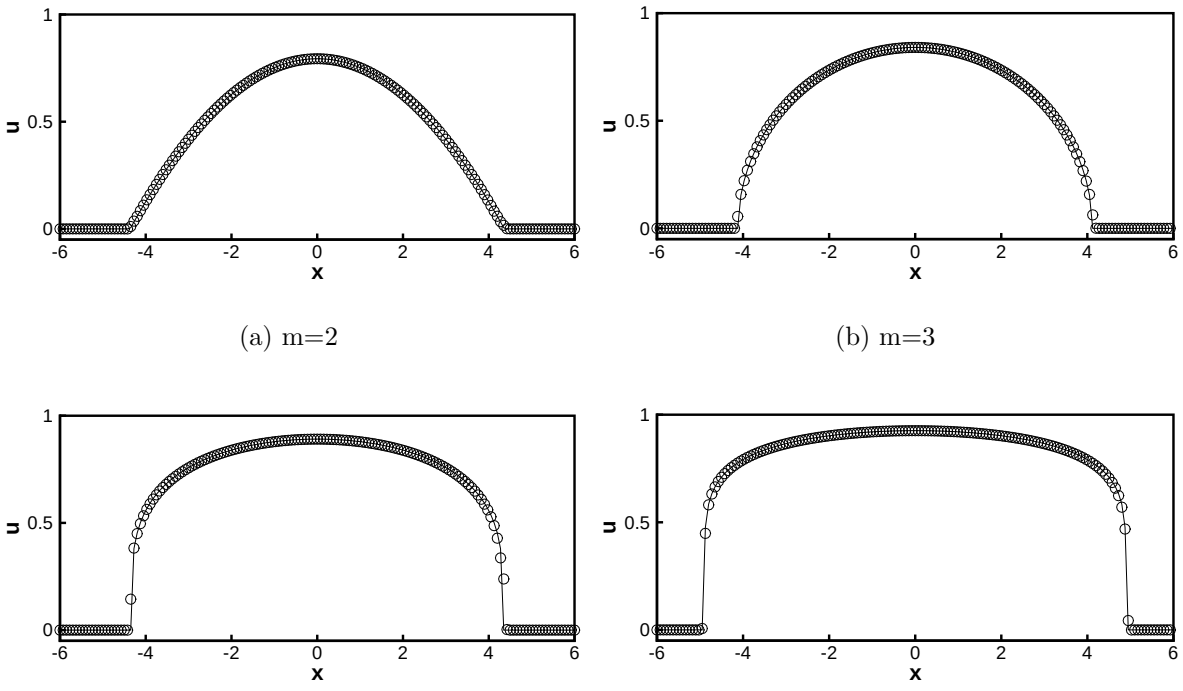

(a) m=2 (b) m=3

(c) m=5 (d) m=8

Figure 2.1: Barenblatt solution for the porous medium equation (1.2). T=2.

We observe that our finite difference WENO scheme can simulate the Barenblatt solution accurately and sharply, without noticeable oscillations near the interface.

Example 3. We now consider the collision of the two-box solution with the same or different heights. If the variable u is regarded as the temperature, the model case is used to describe how the temperature changes when two hot spots are suddenly put in the computational domain.

In Figure 2.2, we plot the evolution of the numerical solution for the PME with $m = 5$ and the initial condition being the two-box solution with the same height

$$u(x,0) = \begin{cases} 1, & \text{if } x \in (-3.7,-0.7) \cup (0.7,3.7), \\ 0, & \text{otherwise.} \end{cases} \tag{2.51}$$

The boundary condition is $u(\pm 5.5, t) = 0$ for $t > 0$, and the computational domain $[-5.5, 5.5]$ is divided into $N = 160$ uniform cells.

We also consider the collision of the two-box solution with different heights. Figure

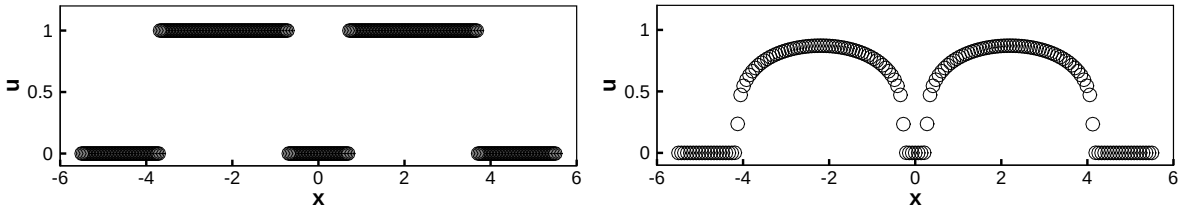

(a) T=0.0

(b) T=0.3

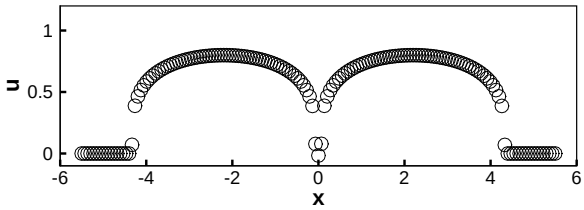

(c) T=0.6

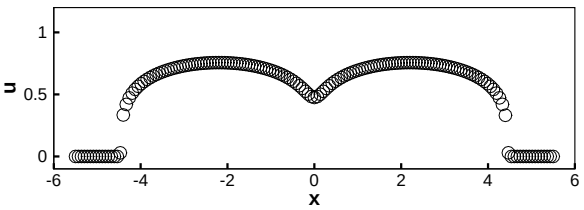

(d) T=0.9

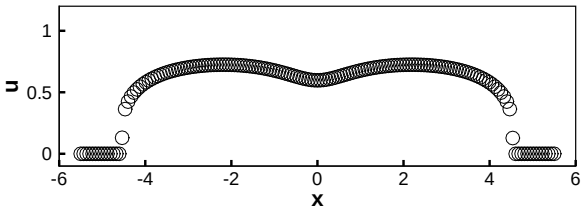

(e) T=1.2

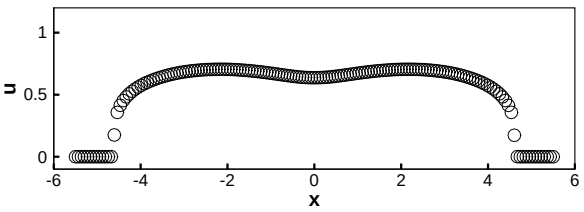

(f) T=1.5

Figure 2.2: Collision of the two-box solution with the same height.

2.3 is the evolution of the numerical solution for the PME with $m = 6$. The initial condition is

$$u(x,0) = \begin{cases} 1, & \text{if } x \in (-4,-1), \\ 2, & \text{if } x \in (0,3), \\ 0, & \text{otherwise.} \end{cases} \tag{2.52}$$

The boundary condition is $u(\pm 6, 0) = 0$ for $t > 0$, and the computational domain is divided into $N = 160$ uniform cells.

From Figures 2.2 and 2.3, we could see that whether the heights of the two boxes in the initial condition are the same or not, the two-box solutions first move outward independently before the collision, then they join each other to make the temperature smooth, and finally the solution becomes almost constant in the common support, agreeing with the results in [32].

Example 4. Next we consider the scalar convection-diffusion Buckley-Leverett equation introduced in [18]

$$u_t + f(u)_x = \varepsilon(\nu(u)u_x)_x, \quad \varepsilon\nu(u) \geq 0. \tag{2.53}$$

This is a prototype model for oil reservoir simulations (two-phase flow). In our test we take $\varepsilon = 0.01$, $f(u)$ to have a s-shaped form

$$f(u) = \frac{u^2}{u^2 + (1-u)^2}, \tag{2.54}$$

and

$$\nu(u) = 4u(1-u). \tag{2.55}$$

The initial function is

$$u(x,0) = \begin{cases} 1 - 3x, & 0 \leq x \leq \frac{1}{3}, \\ 0, & \frac{1}{3} < x \leq 1. \end{cases} \tag{2.56}$$

and the boundary condition is $u(0,t) = 1$.

With the Lax-Friedrichs flux splitting, we apply the fifth order finite difference WENO scheme [15] to approximate the convection term. The numerical solution computed for different number of grid points is shown in Figure 2.4. The numerical results seem to

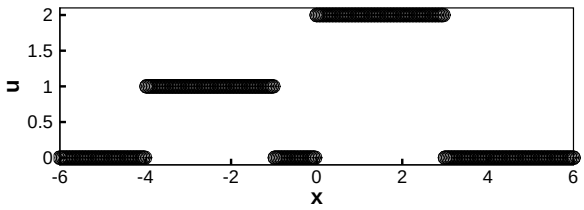

(a) T=0.0

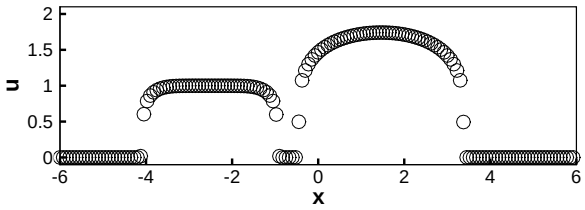

(b) T=0.01

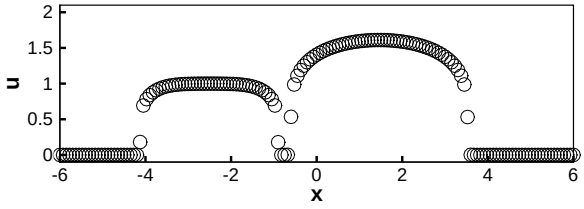

(c) T=0.02

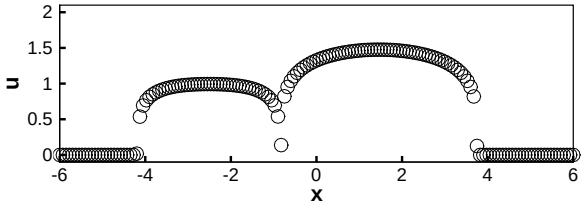

(d) T=0.04

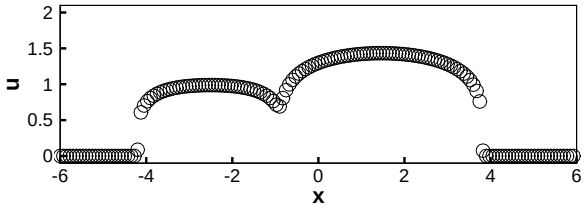

(e) T=0.05

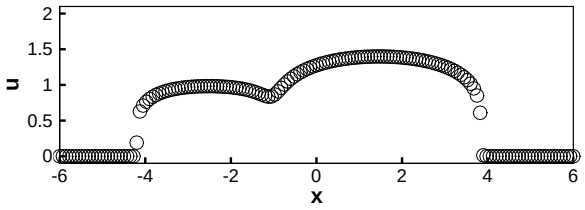

(f) T=0.06

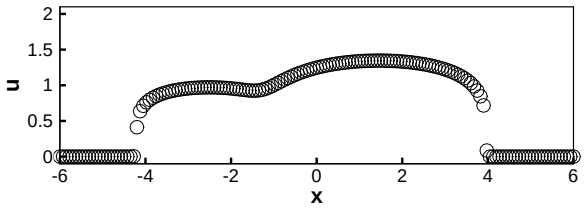

(g) T=0.08

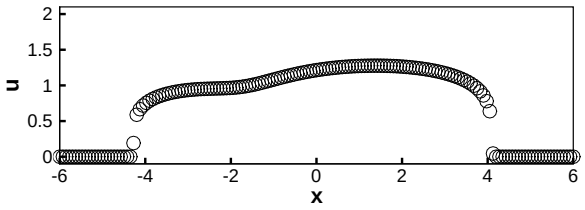

(h) T=0.12

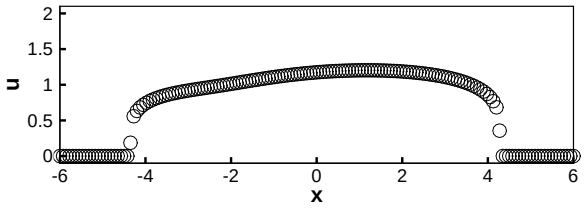

(i) T=0.2

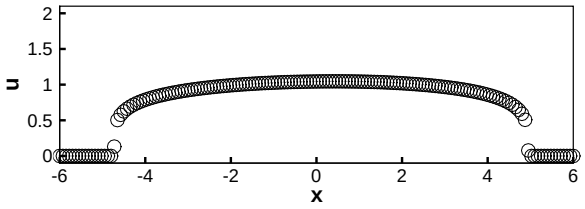

(j) T=0.8

Figure 2.3: Collision of the two-box solution with different heights.

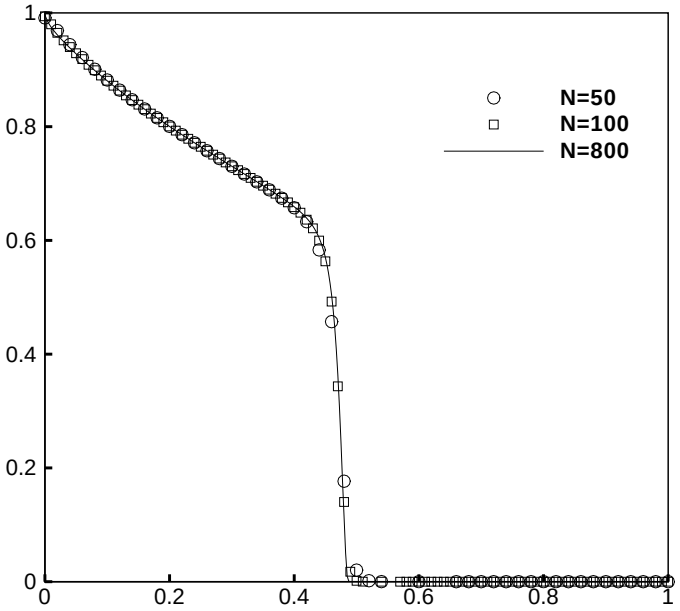

Figure 2.4: Initial-boundary value problem (2.53)-(2.56). T=0.2.

converge to the correct entropy solution nicely, compared with the numerical solutions in [18].

Example 5. Now we consider the Buckley-Leverett equation (2.53) with $\varepsilon = 0.01$, the same diffusion coefficient (2.55) and the flux function $f(u)$ with gravitational effects

$$f(u) = \frac{u^2}{u^2 + (1-u)^2}(1 - 5(1-u)^2). \tag{2.57}$$

We again use the fifth order finite difference WENO scheme [15] to approximate the convection term with the Lax-Friedrichs splitting. The numerical solutions to the problem (2.57) and to the problem (2.53)-(2.55) with the initial condition

$$u(x,0) = \begin{cases} 0, & 0 \le x < 1 - \frac{1}{\sqrt{2}}, \\ 1, & 1 - \frac{1}{\sqrt{2}} \le x \le 1 \end{cases}$$

are shown in Figure 2.5.

Figure 2.5 shows that the finite difference WENO scheme produces numerical solutions accurately without noticeable oscillations for both of the Riemann problems with and without gravitational effects. The results compare well with those in [18].

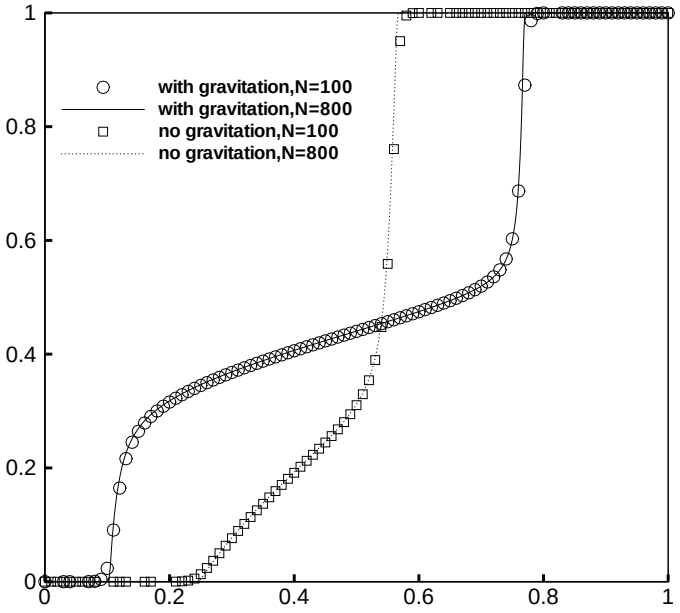

Figure 2.5: Riemann problem for the Buckley-Leverett equation with and without gravitation. T=0.2.

Example 6. Next we consider a one-dimensional model for the glacier growth [12, 17]. The evolution of a glacier of height $h(x,t)$ resting upon a flat mountain could be described by the following nonhomogeneous convection-diffusion equation

$$h_t + f(h)_x = \varepsilon(\nu(h)h_x)_x + S(x,t,h) \tag{2.58}$$

with $\varepsilon = 0.01$ and

$$f(h) = \frac{h+3h^6}{4}, \qquad \nu(h) = 3h^6. \tag{2.59}$$

We solve the Riemann problem with the initial data

$$h(x,0) = \begin{cases} 1, & x < 0, \\ 0, & x > 0 \end{cases}$$

which describes the outlet into a valley disregarding seasonal variations. The source term is taken as $S(x,t,h) = S_0(x)$ if $h(x,t) > 0$, and $S(x,t,h) = \max(S_0(x), 0)$ if $h(x,t) = 0$, where

$$S_0(x) = \begin{cases} 0, & x < -0.4, \\ \frac{1}{2}(x+0.4), & -0.4 \le x \le -0.2, \\ -\frac{1}{2}x, & x > -0.2. \end{cases}$$

The numerical solutions are shown in Figure 2.6 for different numbers of grid points at different times. They seem to converge well with grid refinement and agree well with the results in [17, 18].

Example 7. In this test we consider an example of strongly degenerate parabolic convection-diffusion equation presented in [18]

$$u_t + f(u)_x = \varepsilon(\nu(u)u_x)_x, \quad \varepsilon\nu(u) \geq 0.$$

We take $\varepsilon = 0.1$, $f(u) = u^2$ and

$$\nu(u) = \begin{cases} 0, & |u| \leq 0.25, \\ 1, & |u| > 0.25. \end{cases} \tag{2.60}$$

Therefore the equation is hyperbolic when $u \in [-0.25, 0.25]$ and parabolic elsewhere. We solve the problem with the initial function

$$u(x,0) = \begin{cases} 1, & -\frac{1}{\sqrt{2}} - 0.4 < x < -\frac{1}{\sqrt{2}} + 0.4, \\ -1, & \frac{1}{\sqrt{2}} - 0.4 < x < \frac{1}{\sqrt{2}} + 0.4, \\ 0, & \text{otherwise.} \end{cases} \tag{2.61}$$

The numerical simulations for different numbers of gird points are presented in Figure 2.7, which agree well with the results in [18].

Example 8. Our finite difference WENO scheme (2.46) could also be easily extended to higher dimension, since derivatives in each dimension can be approximated using the one-dimensional point values in that dimension. Here we present a numerical simulation for the two-dimensional porous medium equation

$$u_t = (u^2)_{xx} + (u^2)_{yy}. \tag{2.62}$$

with the initial condition $u_0(x,y)$ given by two bumps

$$u_0(x,y) = \begin{cases} e^{\frac{-1}{6-(x-2)^2-(y+2)^2}}, & (x-2)^2 + (y+2)^2 < 6, \\ e^{\frac{-1}{6-(x+2)^2-(y-2)^2}}, & (x+2)^2 + (y-2)^2 < 6, \\ 0, & \text{otherwise} \end{cases} \tag{2.63}$$

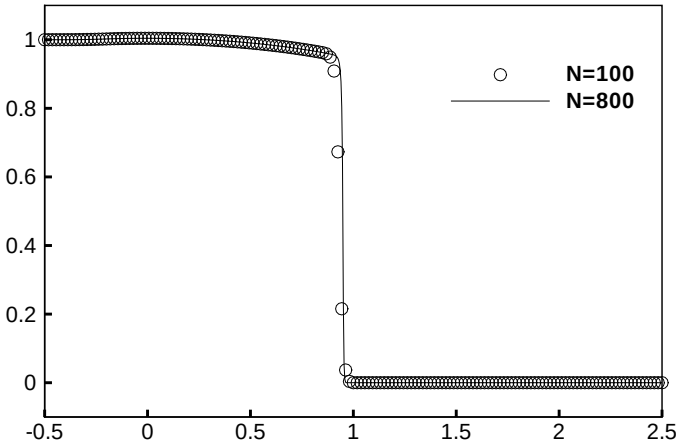

(a) T=1

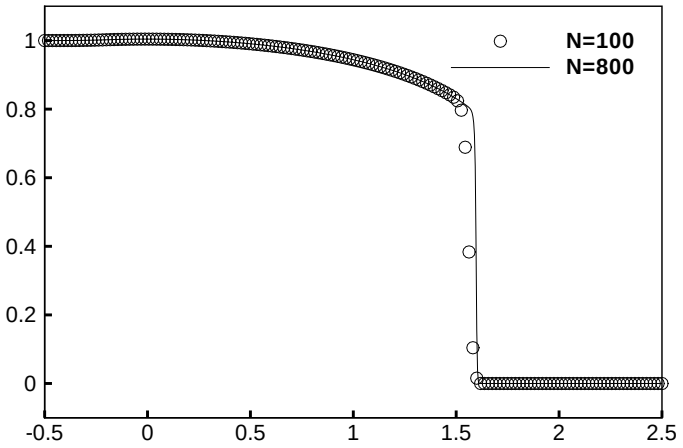

(b) T=2

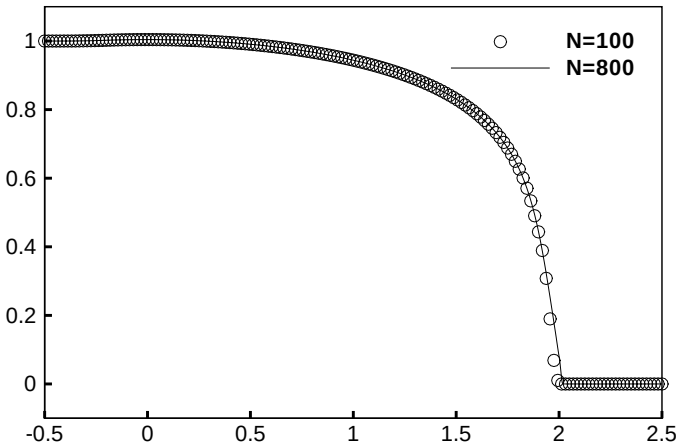

(c) T=4

Figure 2.6: Moving glacier.

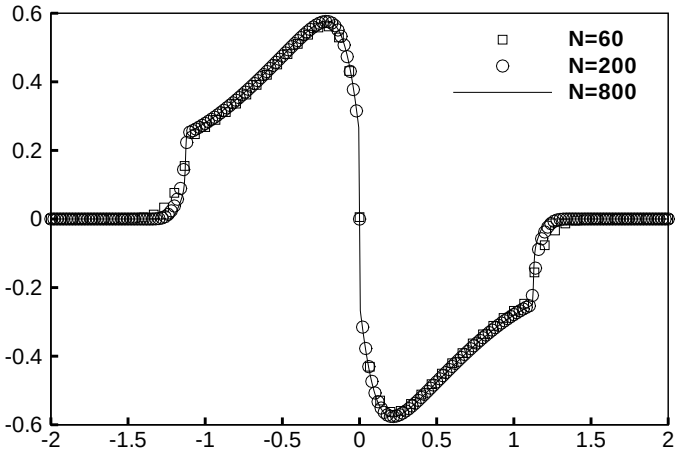

Figure 2.7: Riemann problem (2.53), (2.60) and (2.61). T=0.7.

and periodic boundary conditions on $[-10, 10] \times [-10, 10]$. We compute on the large domain to ensure that the compact support of the solution could still be contained in the computational domain at the final time of the simulation. We show the numerical results at $T = 0$, 0.5, 1.0 and 4.0 in Figure 2.8 from top left to bottom right respectively, with the computational domain $[-10, 10]$ divided into 80×80 uniform cells. The results compare well with those in [7].

Example 9. Consider the two-dimensional extension of the equation in Example 7 given in [18]

$$u_t + f(u)_x + f(u)_y = \varepsilon(\nu(u)u_x)_x + \varepsilon(\nu(u)u_y)_y$$

with $\varepsilon = 0.1$, $f(u) = u^2$ and $\nu(u)$ given in (2.60). The initial data are equal to -1 and 1 inside two circles of radius 0.4 centered at $(0.5, 0.5)$ and $(-0.5, -0.5)$ respectively and zero elsewhere inside the square $[-1.5, 1.5] \times [-1.5, 1.5]$. The numerical simulation is presented in Figure 2.9, which compares well with that in [18].

3 Rewriting in a system

In Section 2, we have shown the direct approximation to the second derivative in detail and have presented the numerical results to demonstrate the high order accuracy and the non-oscillatory performance. Now we would like to use the idea of the local discontinuous

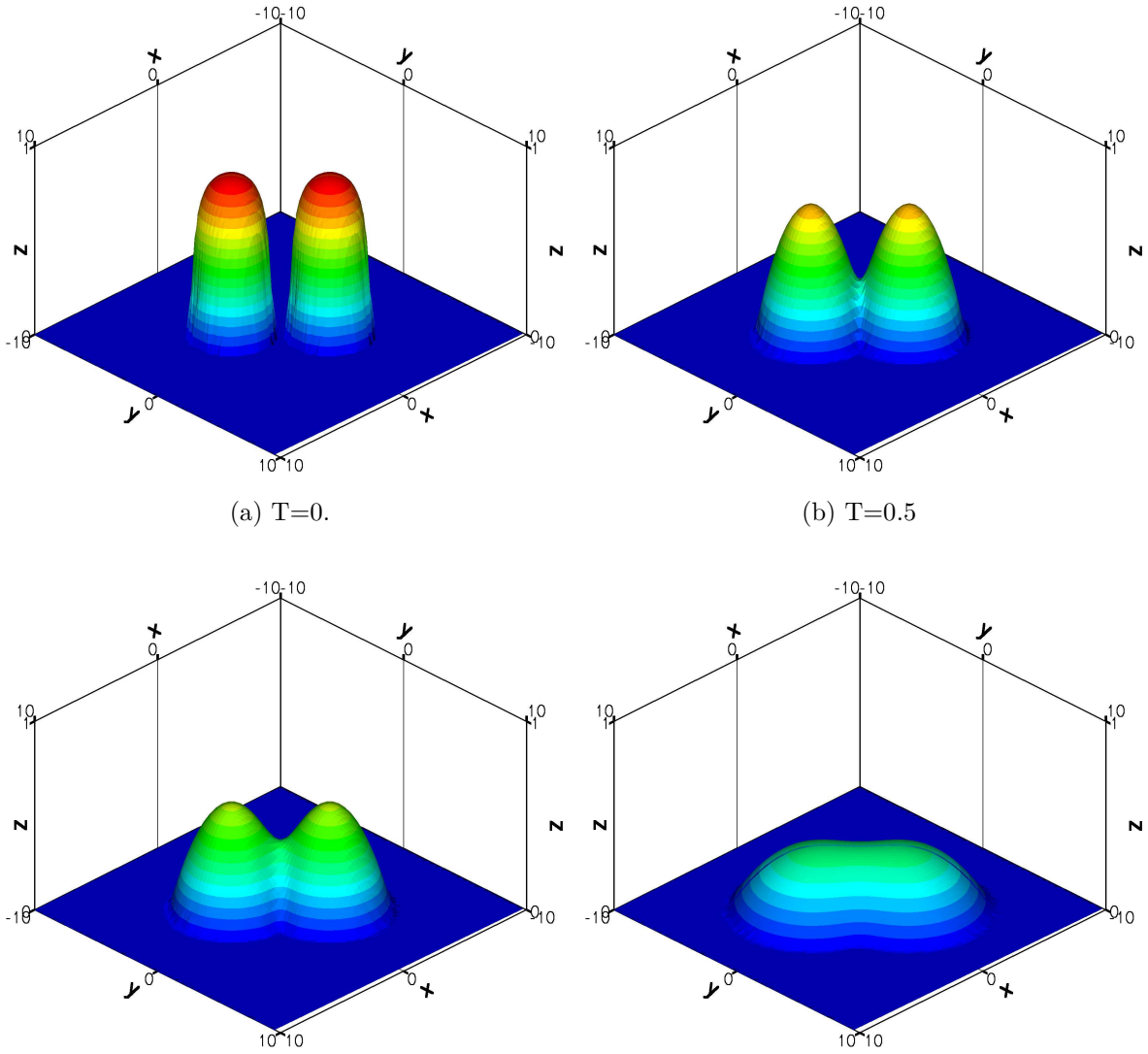

(a) T=0. (b) T=0.5

(c) T=1.0 (d) T=4.0

Figure 2.8: The numerical solution of the porous medium equation in 2D.

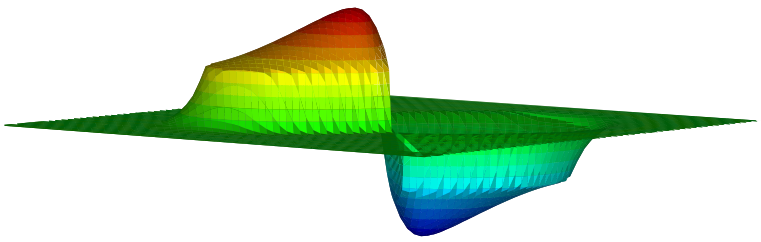

Figure 2.9: Degenerate parabolic problem-solution at time T=0.5 on a 60×60 grid.

Galerkin method [10], to first rewrite the equation (1.1) as a nonlinear system of first order equations

$$u_t = v_x, \tag{3.1}$$

$$v = b(u)_x \tag{3.2}$$

and then to solve the two first order equations respectively using the fifth order finite difference WENO method for conservation laws [15]. In order to make the final effective stencil smaller, we use a right-biased stencil for (3.1) followed by a left-biased stencil for (3.2).

3.1 Approximation to two first derivatives

3.1.1 Approximation to the second equation (3.2)

Based on the left-biased big stencil $S = \{x_{i-2}, \ldots, x_{i+2}\}$, assuming the grid is uniform, i.e. $\Delta x = x_{i+1} - x_i$ is a constant, we first solve the equation (3.2) using the finite difference approximation and writing it in a conservative form

$$v_i = \frac{\hat{g}_{i+\frac{1}{2}} - \hat{g}_{i-\frac{1}{2}}}{\Delta x}. \tag{3.3}$$

Given the point values of the function $b(u(x))$, the problem we face now is to find a numerical flux function

$$\hat{g}_{i+\frac{1}{2}} = \hat{g}(u_{i-2}, \ldots, u_{i+2}) \tag{3.4}$$

such that the flux difference approximates the first order derivative $b(u(x))_x$ at $x = x_i$ to fifth order accuracy

$$\frac{\hat{g}_{i+\frac{1}{2}} - \hat{g}_{i-\frac{1}{2}}}{\Delta x} = (b(u))_x|_{x=x_i} + O(\Delta x^5). \tag{3.5}$$

This is the standard problem for solving conservation laws [15]. We therefore only list the results here.

We could obtain the flux $\hat{g}_{i+\frac{1}{2}}$ based on the big stencil as

$$\hat{g}_{i+\frac{1}{2}} = \frac{2b(u_{i-2}) - 13b(u_{i-1}) + 47b(u_i) + 27b(u_{i+1}) - 3b(u_{i+2})}{60}. \tag{3.6}$$

Similarly, we could evaluate the three different fluxes

$$\begin{aligned}
\hat{g}^{(0)}_{i+\frac{1}{2}} &= \frac{2b(u_{i-2}) - 7b(u_{i-1}) + 11b(u_i)}{6}, \\
\hat{g}^{(1)}_{i+\frac{1}{2}} &= \frac{-b(u_{i-1}) + 5b(u_i) + 2b(u_{i+1})}{6}, \\
\hat{g}^{(2)}_{i+\frac{1}{2}} &= \frac{2b(u_i) + 5b(u_{i+1}) - b(u_{i+2})}{6},
\end{aligned} \tag{3.7}$$

which are based on the three small stencils $S^m = \{x_{i-2+m}, x_{i-1+m}, x_{i+m}\}$ with $m = 0, 1, 2$ respectively.

The linear weights d_m with $m = 0, 1, 2$ are given by

$$d_0 = \frac{1}{10}, \qquad d_1 = \frac{3}{5}, \qquad d_2 = \frac{3}{10},$$

satisfying $\hat{g}_{i+\frac{1}{2}} = \sum_{m=0}^{2} d_m \hat{g}^{(m)}_{i+\frac{1}{2}}$ and the consistence condition $\sum_{m=0}^{2} d_m = 1$. The smoothness indicators are given by

$$\begin{aligned}
\beta_0 &= \frac{13}{12}(b(u_{i-2}) - 2b(u_{i-1}) + b(u_i))^2 + \frac{1}{4}(b(u_{i-2}) - 4b(u_{i-1}) + 3b(u_i))^2, \\
\beta_1 &= \frac{13}{12}(b(u_{i-1}) - 2b(u_i) + b(u_{i+1}))^2 + \frac{1}{4}(b(u_{i-1}) - b(u_{i+1}))^2, \\
\beta_2 &= \frac{13}{12}(b(u_i) - 2b(u_{i+1}) + b(u_{i+2}))^2 + \frac{1}{4}(3b(u_i) - 4b(u_{i+1}) + b(u_{i+2}))^2.
\end{aligned} \tag{3.8}$$

Therefore we discretize the equation (3.2) on the left-biased big stencil $S = \{x_{i-2}, \ldots, x_{i+2}\}$ in the form (3.3), where the flux is constructed as follows

$$\hat{g}_{i+\frac{1}{2}} = \sum_{m=0}^{2} \omega_m \hat{g}^{(m)}_{i+\frac{1}{2}} \tag{3.9}$$

with $\hat{g}^{(m)}_{i+\frac{1}{2}}$ given in (3.7) and the nonlinear weights defined by

$$\omega_m = \frac{\alpha_m}{\sum_{j=0}^{2} \alpha_j}, \qquad \alpha_m = \frac{d_m}{(\epsilon + \beta_m)^2}, \qquad m = 0, 1, 2. \tag{3.10}$$

Here ϵ is again taken as 10^{-6}. The smoothness indicators β_m with $m = 0, 1, 2$ are given in (3.8).

3.1.2 Approximation to the first equation (3.1)

In Section 3.1.1, we have obtained the point values of the function $v(x)$ in (3.2). We can use the previous reconstruction again to get the numerical flux $\hat{f}_{i+\frac{1}{2}}$ for solving the equation (3.1) based on the right-biased big stencil $S = \{x_{i-1}, \ldots, x_{i+3}\}$, written in the form

$$\frac{du_i(t)}{dt} = \frac{\hat{f}_{i+\frac{1}{2}} - \hat{f}_{i-\frac{1}{2}}}{\Delta x}. \tag{3.11}$$

Following a similar argument as in the previous section, we could obtain the fluxes

$$\begin{aligned} \hat{f}^{(0)}_{i+\frac{1}{2}} &= \frac{-v_{i-1} + 5v_{i-1} + 2v_i}{6}, \\ \hat{f}^{(1)}_{i+\frac{1}{2}} &= \frac{2v_i + 5v_{i+1} - v_{i+2}}{6}, \\ \hat{f}^{(2)}_{i+\frac{1}{2}} &= \frac{11v_i - 7v_{i+2} + 2v_{i+3}}{6}, \end{aligned} \tag{3.12}$$

the linear weights

$$d_0 = \frac{3}{10}, \qquad d_1 = \frac{3}{5}, \qquad d_2 = \frac{1}{10},$$

and the nonlinear weights defined by

$$\omega_m = \frac{\alpha_m}{\sum_{j=0}^{2} \alpha_j}, \qquad \alpha_m = \frac{d_m}{(\epsilon + \beta_m)^2}, \qquad m = 0, 1, 2, \tag{3.13}$$

based on the three small stencils $S^m = \{x_{i-1+m}, x_{i+m}, x_{i+1+m}\}$ with $m = 0, 1, 2$ respectively. Here the smooth indicators β_m are

$$\begin{aligned} \beta_0 &= \frac{13}{12}(v_{i-1} - 2v_i + v_{i+1})^2 + \frac{1}{4}(v_{i-1} - 4v_i + 3v_{i+1})^2, \\ \beta_1 &= \frac{13}{12}(v_i - 2v_{i+1} + v_{i+2})^2 + \frac{1}{4}(v_i - v_{i+2})^2, \\ \beta_2 &= \frac{13}{12}(v_{i+1} - 2v_{i+2} + v_{i+3})^2 + \frac{1}{4}(3v_{i+1} - 4v_{i+2} + v_{i+3})^2. \end{aligned} \tag{3.14}$$

Finally on the right-biased big stencil $S = \{x_{i-1}, \ldots, x_{i+3}\}$ we obtain the numerical flux for the fifth finite difference WENO scheme (3.11)

$$\hat{f}_{i+\frac{1}{2}} = \sum_{m=0}^{2} \omega_m \hat{f}^{(m)}_{i+\frac{1}{2}} \tag{3.15}$$

where ω_m and $\hat{f}^{(m)}_{i+\frac{1}{2}}$ are given in (3.13) and (3.12) respectively.

Table 3.1: Accuracy on $u_t = u_{xx}$ with $u(x,0) = \sin(x)$

N	L^1 error	order	L^∞ error	order
10	6.05E-03	–	2.63E-03	–
20	1.13E-04	5.74	4.25E-05	5.95
40	1.78E-06	5.99	7.08E-07	5.91
80	2.62E-08	6.08	1.12E-08	5.98
160	3.95E-10	6.05	1.73E-10	6.01
320	4.74E-12	6.38	2.74E-12	5.98

3.2 Numerical results for the PME

For the time discretization, we still use the same third order TVD Runge-Kutta method given in Section 2.2.4.

Example 10. Similarly we first test the accuracy of the finite difference WENO scheme constructed in (3.3) and (3.11) for the case $m = 1$ in (1.2), that is the linear problem with the smooth initial condition (2.50). Table 3.1 shows the results at the final time $T = 2$ with periodic boundary condition.

We could see that this second WENO method also achieves sixth order accuracy, however its error magnitude is larger than that of the first WENO method in the previous section on the same mesh. Notice that the second WENO method also involves more computation and has a larger effective stencil.

Example 11. Now we compute the Barenblatt solution given in (1.3) of the PME (1.2), with the initial condition taken as the Barenblatt solution at $t = 1$, and the boundary condition $u(\pm 6, t) = 0$ for $t > 1$.

Dividing the computational domain into $N = 160$ uniform cells, we plot the numerical solution at $T = 2$ respectively for $m = 2, 3, 5$ and 8. The circle-box is the numerical solution and the solid line is the exact solution.

We could observe that by rewriting the PME as a system, the finite difference WENO scheme can also simulate the Barenblatt solution accurately and sharply, without noticeable oscillations near the interface.

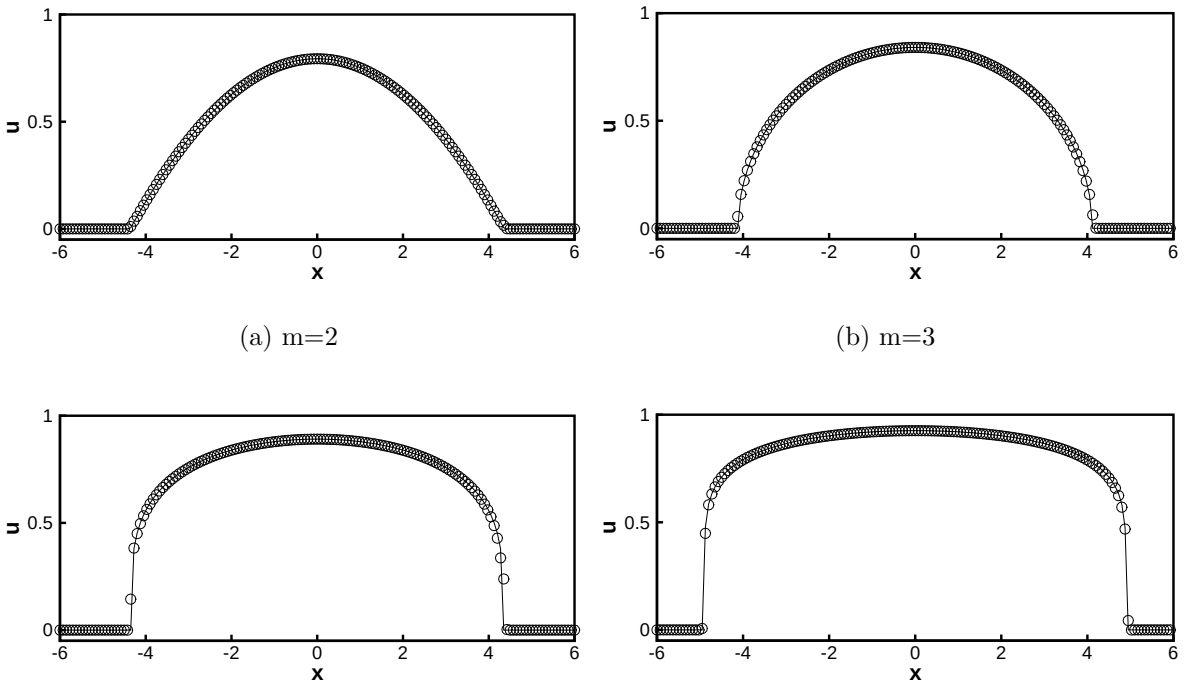

(a) m=2 (b) m=3

(c) m=5 (d) m=8

Figure 3.1: Numerical results by rewriting in a system. T=2.

We have also applied the second WENO scheme in this section to Examples 3 to 9 in the previous section, obtaining equally good non-oscillatory solutions. We will not present the results here to save space.

4 Concluding remarks

In this paper we consider two different formulations of WENO schemes for approximating possibly degenerate parabolic equations. The first formulation approximates directly the second derivative term using a conservative flux difference and the second approach applies the WENO procedure to two first order equations using the idea of the local discontinuous Galerkin method. Both of the numerical methods could achieve high order accuracy and can simulate discontinuous solutions without oscillations. Comparing Table 2.2 and Table 3.1, we observe that even though both of them could achieve sixth order accuracy, the first method has a smaller error magnitude on the same mesh.

References

[1] D. Aregba-Driollet, R. Natalini, and S. Tang, *Explicit diffusive kinetic schemes for nonlinear degenerate parabolic systems*, Mathematics of Computation, 73 (2004), 63-94.

[2] D.G. Aronson, *The porous medium equation*, in *Nonlinear Diffusion Problems*, Lecture Notes in Mathematics, Springer Berlin, 1224 (1986), 1-46.

[3] D. Balsara and C.-W. Shu, *Monotonicity preserving weighted essentially non-oscillatory schemes with increasingly high order of accuracy*, Journal of Computational Physics, 160 (2000), 405-452.

[4] G.I. Barenblatt, *On self-similar motions of compressible fluid in a porous medium*, Prikl. Mat. Mekh., 16 (1952), 679-698 (in Russian).

[5] A.E. Berger, H. Brezis and J.C. Rogers, *A numerical method for solving the problem* $u_t - \Delta f(u) = 0$, RAIRO Numerical Analysis, 13 (1979), 297-312.

[6] E. Carlini, R. Ferretti and G. Russo, *A weighted essentially nonoscillatory, large time-step scheme for Hamilton-Jacobi equations*, SIAM Journal on Scientific Computing, 27 (2005), 1071-1091.

[7] F. Cavalli, G. Naldi, G. Puppo and M. Semplice, *High order relaxation schemes for nonlinear degenerate diffusion problems*, SIAM Journal on Numerical Analysis, 45 (2007), 2098-2119.

[8] C.-S. Chou and C.-W. Shu, *High order residual distribution conservative finite difference WENO schemes for steady state problems on non-smooth meshes*, Journal of Computational Physics, 214 (2006), 698-724.

[9] C.-S. Chou and C.-W. Shu, *High order residual distribution conservative finite difference WENO schemes for convection-diffusion steady state problems on non-smooth meshes*, Journal of Computational Physics, 224 (2007), 992-1020.

[10] B. Cockburn and C.-W. Shu, *The local discontinuous Galerkin method for time-dependent convection-diffusion systems*, SIAM Journal on Numerical Analysis, 35 (1998), 2440-2463.

[11] S. Evje and K. H. Karlsen, *Viscous splitting approximation of mixed hyperbolic-parabolic convection-diffusion equations*, Numerische Mathematik, 83(1999), 107-137.

[12] A.C. Flower, *Glaciers and ice sheets*, in *The Mathematics of Model for Climatology and Environment*, edited by J.I. Diaz, NATO ASI Series, Springer-Verlag, Berlin/New York, 48 (1996), 302-336.

[13] A.K. Henrick, T.D. Aslam and J.M. Powers, *Mapped weighted essentially non-oscillatory schemes: Achieving optimal order near critical points*, Journal of Computational Physics, 207 (2005), 542-567.

[14] W. Jäger and J. Kačur, *Solution of porous medium type systems by linear approximation schemes*, Numerische Mathematik, 60 (1991), 407-427.

[15] G. Jiang and C.-W. Shu, *Efficient implementation of weighted ENO schemes*, Journal of Computational Physics, 126 (1996), 202-228.

[16] J. Kačur, A. Handlovičová, and M. Kačurová, *Solution of nonlinear diffusion problems by linear approximation schemes*, SIAM Journal on Numerical Analysis, 30 (1993), 1703-1722.

[17] K.H. Karlsen and K.A. Lie, *An unconditionally stable splitting for a class of nonlinear parabolic equations*, IMA Journal of Numerical Analysis, 19 (1999), 609-635.

[18] A. Kurganov and E. Tadmor, *New high-resolution central schemes for nonlinear conservation laws and convection-diffusion equations*, Journal of Computational Physics, 160 (2000), 241-282.

[19] X.-D. Liu, S. Osher and T. Chan, *Weighted essentially non-oscillatory schemes*, Journal of Computational Physics, 115 (1994), 200-212.

[20] Y. Liu, C.-W. Shu and M. Zhang, *On the positivity of linear weights in WENO approximations*, Acta Mathematicae Applicatae Sinica, 25 (2009), 503-538.

[21] E. Magenes, R.H. Nochetto, and C. Verdi, *Energy error estimates for a linear scheme to approximate nonlinear parabolic problems*, RAIRO Mathematical Modelling and Numerical Analysis, 21 (1987), 655-678.

[22] M. Muskat, *The flow of homogeneous fluids through porous media*, McGraw-Hill Book Co., New York, 1937.

[23] R.H. Nochetto, A. Schmidt and C. Verdi, *A posteriori error estimation and adaptivity for degenerate parabolic problems*, Mathematics of Computation, 69 (2000), 1-24.

[24] R.H. Nochetto, and C. Verdi, *Approximation of degenerate parabolic problems using numerical integration*, SIAM Journal on Numerical Analysis, 25 (1988), 784-814.

[25] I.S. Pop and W. Yong, *A numerical approach to degenerate parabolic equations*, Numerische Mathematik, 92 (2002), 357-381.

[26] K. Sebastian and C.-W. Shu, *Multi domain WENO finite difference method with interpolation at sub-domain interfaces*, Journal of Scientific Computing, 19 (2003), 405-438.

[27] J. Shi, C. Hu and C.-W. Shu, *A technique of treating negative weights in WENO schemes*, Journal of Computational Physics, 175 (2002), 108-127.

[28] C.-W. Shu, *Essentially non-oscillatory and weighted essentially non-oscillatory schemes for hyperbolic conservation laws*, in *Advanced Numerical Approximation of Nonlinear Hyperbolic Equations*, B. Cockburn, C. Johnson, C.-W. Shu and E. Tadmor (Editor: A. Quarteroni), Lecture Notes in Mathematics, Springer, 1697 (1998), 325-432.

[29] C.-W. Shu, *High order weighted essentially non-oscillatory schemes for convection dominated problems*, SIAM Review, 51 (2009), 82-126.

[30] C.-W. Shu and S. Osher, *Efficient implementation of essentially non-oscillatory shock-capturing schemes*, Journal of Computational Physics, 77 (1988), 439-471.

[31] Ya.B. Zel'dovich and A.S. Kompaneetz, *Towards a theory of heat conduction with thermal conductivity depending on the temperature*, in Collection of papers dedicated to 70th Anniversary of A.F. Ioffe, Izd. Akad. Nauk SSSR, Moscow, 1950, 61-72.

[32] Q. Zhang and Z. Wu, *Numerical simulation for porous medium equation by local discontinuous Galerkin finite element method*, Journal of Scientific Computing, 38 (2009), 127-148.